Hindawi
Advances in Materials Science and Engineering
Volume 2023, Article ID 9870519, 1 page
https://doi.org/10.1155/2023/9870519

Retraction

Retracted: Wind Tunnel Testing and Validation of Helicopter Rotor Blades Using Additive Manufacturing

Advances in Materials Science and Engineering

Received 26 December 2023; Accepted 26 December 2023; Published 29 December 2023

This article has been retracted by Hindawi, as publisher, following an investigation undertaken by the publisher [1]. This investigation has uncovered evidence of systematic manipulation of the publication and peer-review process. We cannot, therefore, vouch for the reliability or integrity of this article.

Please note that this notice is intended solely to alert readers that the peer-review process of this article has been compromised.

Wiley and Hindawi regret that the usual quality checks did not identify these issues before publication and have since put additional measures in place to safeguard research integrity.

We wish to credit our Research Integrity and Research Publishing teams and anonymous and named external researchers and research integrity experts for contributing to this investigation.

The corresponding author, as the representative of all authors, has been given the opportunity to register their agreement or disagreement to this retraction. We have kept a record of any response received.

References

[1] I. Hasan, R. Mukesh, P. Radha Krishnan, R. Srinath, D. P. Babu, and N. Lemma Gurmu, "Wind Tunnel Testing and Validation of Helicopter Rotor Blades Using Additive Manufacturing," *Advances in Materials Science and Engineering*, vol. 2022, Article ID 4052208, 13 pages, 2022.

Hindawi
Advances in Materials Science and Engineering
Volume 2022, Article ID 4052208, 13 pages
https://doi.org/10.1155/2022/4052208

Research Article

Wind Tunnel Testing and Validation of Helicopter Rotor Blades Using Additive Manufacturing

Inamul Hasan,[1,2] **R. Mukesh**,[3] **P. Radha Krishnan**,[1,2] **R. Srinath**,[2,4] **Dhanya Prakash Babu**,[1] **and Negash Lemma Gurmu**[5]

[1]*Department of Aeronautical Engineering, ACS College of Engineering, Bangalore 560074, Karnataka, India*
[2]*Department of Aeronautical Engineering, Visvesvaraya Technological University, Belagavi 590018, Karnataka, India*
[3]*Department of Aerospace Engineering, ACS College of Engineering, Bangalore 560074, Karnataka, India*
[4]*Department of Aerospace Engineering, Dayananda Sagar University, Bangalore 560078, Karnataka, India*
[5]*Department of Industrial Engineering, Ambo University, Ambo, Ethiopia*

Correspondence should be addressed to Negash Lemma Gurmu; negash.lemma@ambou.edu.et

Received 24 June 2022; Revised 2 August 2022; Accepted 20 August 2022; Published 21 September 2022

Academic Editor: K. Raja

This research paper aims to validate the aerodynamic performance of rotor blades using additive manufacturing techniques. Wind tunnel testing is a technique used to find the flow characteristics of the body. Computational fluid dynamics (CFD) techniques are used for aerodynamic analysis, and validation should be done using wind tunnel testing. In the aerodynamic testing of models, additive manufacturing techniques help in validating the results by making models easily for wind tunnels. Recent developments in additive manufacturing help in the aerodynamic testing of models in wind tunnels. The CFD analysis of helicopter rotor blades was analyzed in this research, and validation was done using additive manufacturing techniques. Computational analysis was carried out for static analysis for the forward speeds of Mach numbers 0.3, 0.4, and 0.5. The results obtained were satisfactory to the previous results and were validated with wind tunnel testing. Results proved that the error percentage was lower, and the computational analysis was valid. In this research, models were designed using the FDM technique for wind tunnel testing as it is cost-effective and easy to manufacture.

1. Introduction

A helicopter is a flying machine with many advantages over other flying objects, such as landing or take-off at almost any terrain, flying at a specific position (hovering), and flying backward and sidewards quickly. Helicopters can be termed any terrain vehicle as they have many advantages over aircraft [1, 2]. The helicopter is a type of rotorcraft currently used for many purposes such as rescue, firefighting, and agriculture. The helicopter's design differs with various parameters for different applications [3]. Helicopters possess more capability than aircraft as it has the unique ability of vertical take-off and landing, and no particular runway. Helicopters have some disadvantages over aircraft in the case of speed and pilot operation. The helicopter speed is improved since the invention of the helicopter in recent days. Many factors are suppressing the speed of helicopters [4]. Helicopters can fly forward, backward, or sideways, stay at a position (hover), and vertically can go up or come down. In aircraft, lift is produced by the wings, and engines produce thrust. In helicopters, lift and thrust are produced by a rotor driven by one or two engines [5, 6].

CFD software is used for analyzing the aerodynamic performance of moving vehicles to assess the aerodynamic performance. CFD is widely used in many fields, and improving CFD techniques helps improve results and reduce errors [7]. Even though CFD software provides good results, researchers prefer to compare the results obtained from CFD with wind tunnel testing. CFD results can be validated with the previous experimental results or wind tunnel tests [8, 9]. The model was made from wood or metals for wind tunnel tests in the previous days. Models created in wood require a

high cost for skilled workers, and it takes a long time to make the models. Metals like aluminum were used to prepare the model using CNC machines are high cost and less affordable [10, 11].

The evolution of additive manufacturing techniques helps in the easy and affordable manufacturing of models for various applications. Mainly for wind tunnel testing with the help of CAD design software, it is easy to design and manufacture with less cost [12, 13]. Advancements in additive manufacturing technologies help many fields in engineering, medicine, and research to test or demonstrate the models [14, 15]. Material qualities are improved by the advancements in the development of composite materials and help make low-cost models faster [16].

2. Experimental Details

2.1. CFD Analysis. Four-bladed helicopters are chosen as it is used in most high-speed helicopters. Analysis was carried out by ANSYS fluent software. It provides the numerical solution computationally with the help of the Navier–Stokes equation over the flow region. These computational techniques are beneficial for research on complex problems. Four-bladed rotors are designed by CATIA V5 software. Coordinates are downloaded from the UIUC airfoil data site, and the 2D profile can be generated from the airfoil data [17].

2.1.1. Design and Preprocessing. The CAD model design is essential and a preliminary requirement for computational analysis. CAD models can be designed by any design software like Solid Works, Solid Edge, and Catia. [18]. Catia V5 is used in this research work to design the three-bladed and four-bladed helicopter blades. The same model is used for the experimental model and scaled down for wind tunnel size using the 3D printing method [19, 20]. The designed model will be imported to fluent for further analysis. After designing the model, the model is imported to the ANSYS CFD workbench for further processing and analysis. The first stage is preprocessing, where the meshing and boundary conditions are applied [21]. As it is a static analysis, C type domain was chosen for computational analysis. Unstructured meshing is chosen as it is a complex structure to provide accurate results in CFD analysis [22, 23]. The realizable k-ε model is chosen as the solver because it provides better results than other models, as mentioned in Figure 1.

The analysis was carried out for all the models and compared with experimental results to finalize the turbulence model. The analysis showed that realizable $k-\varepsilon$ was near the experimental results [22, 24].

An analysis was carried out for HH02 and NASA SC(2)-0714 rotor airfoils for Mach numbers of 0.3, 0.4, and 0.5. Blades are designed with the exact scaling of the Apache helicopter as the HH02 airfoil provides high performance. Parts of the rotors are designed separately as the leading edge, trailing edge, and center part, having a fine mesh for the analysis. Geometric parameters are followed in Table 1. Blade designs are shown in Figures 2 and 3.

Design parameters for the four-bladed configuration are shown in Table 1. Required parameters to design the helicopter blades are mainly rotor solidity and aspect ratio of the wing. Analysis was carried out for the Mach numbers of 0.3, 0.4, and 0.5 as most high-speed helicopters operate at Mach number 0.4. HH02 and NASA SC(2)-0714 rotors were analyzed to obtain the flow characteristics.

2.1.2. Grid Independence Study. The grid independence test was conducted to obtain the correct result for verification. Details of the grid independence test are represented in Table 2. $Y+$ value is maintained at 30 to 50 for all analyses. The number of elements increased, and the lift and drag coefficients were obtained from the numerical results. The grid size is decreased, and the study was carried out until the result variation was less than 2% higher than the previous grid [25, 26]. For the elements of 10921474, the lift coefficient and drag coefficient values showed a 1.47% deviation. So, the number of elements is fixed, and the boundary conditions are applied. The plot showing the variation of lift coefficient with many elements is shown in Figure 4.

3. Wind Tunnel Testing

The wind tunnel is a device used to study and analyze the flow characteristics of any object. The wind tunnel is an essential part of aerodynamics. The wind tunnel used a control stream of air to create an environment where the air flows over the model to study the effects of airflow. Wind tunnel testing is not only applicable to flying vehicles. It is also applicable for automobiles, buildings, or moving or flowing objects [9, 27].

Wind tunnels are classified based on the speed of flow created in the test section. Also, based on the operation, it is classified as open section and closed section wind tunnels.

Wind tunnels for rotorcraft differ from wind tunnels for aircraft or only wing sections. Static analysis can be carried out in any wind tunnel to analyze rotorcraft blade properties in static conditions [28, 29].

This study carried out an open section low-speed subsonic wind tunnel analysis for static analysis of HH02 and NASA SC(2)-0714 rotors.

Lift, drag, and moment can be measured by a three-component balance system attached to the wind tunnel. The three-component balance system directly measures the force and moment with the help of strain gauges inside the balance. In modern wind tunnels, a six-component balance is available to measure lateral force, longitudinal force, vertical force, pitching moment, rolling moment, and yawing moment [30].

The wind tunnel used for testing and force balance measurement and control for wind tunnels are shown in Figures 5(a) and 5(b).

In Figure 6, 3D printed models are shown. Four-bladed models of HH02 and NASA SC(2)-0714 rotors are printed with the FDM method. The NASA SC(2)-0714 rotor is the black colored model, and the HH02 rotor is the white

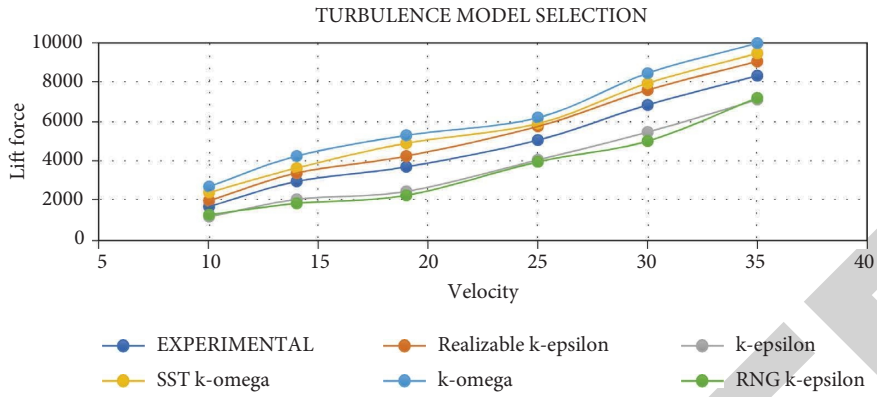

Figure 1: Turbulence model selection.

Table 1: Design parameters for four-bladed analysis.

Parameters	Symbols	HH02	NASA SC(2)-0714
The number of blades	N_b	4	4
Rotor blade radius	R	5.574	5.574
Chord length	C	0.145	0.145
Mach no.	M	0.3, 0.4, 0.5	0.3, 0.4, 0.5
Blade aspect ratio	AR	16.9	16.9
Rotor solidity	σ	0.033	0.033
Blade span (m)	b	5.086	5.086
Blade root chord (m)	Cr	0.3191	0.3191
Blade root chord (m)	Ct	0.0663	0.0663
Blade planform area (m^2)	S	1.5299	1.5299

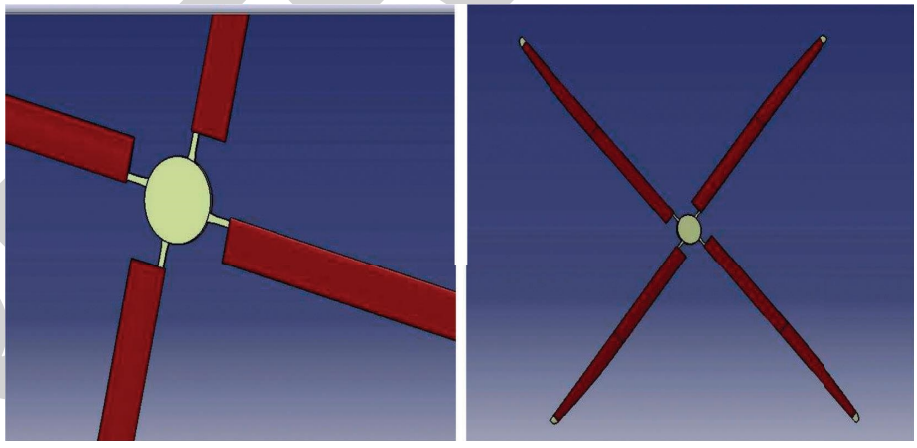

Figure 2: HH02 rotor model.

colored model. The models are used in the wind tunnel for testing in static conditions.

Computational techniques have developed a lot in recent days. But experimental testing is essential for validating the computational results and rectifying the errors [31]. In previous days, making models are not accessible. Wood or steel models should be used for testing in wind tunnels. Nowadays, 3D printing models are developed, and models can be made easily for the requirement.

Wind tunnels are available in various sizes and configurations. The full-scale wind tunnels where a complete aircraft or helicopter can be placed inside the test section. The scaled-down tunnel will have a lesser dimension test section. The actual model should be scaled down based on similarity parameters for scaled-down models. The model is a small one that is scaled-down, and the prototype is a real one with full dimensions. A geometric, kinematic, and dynamic similarity between the model and prototype should exist [32, 33].

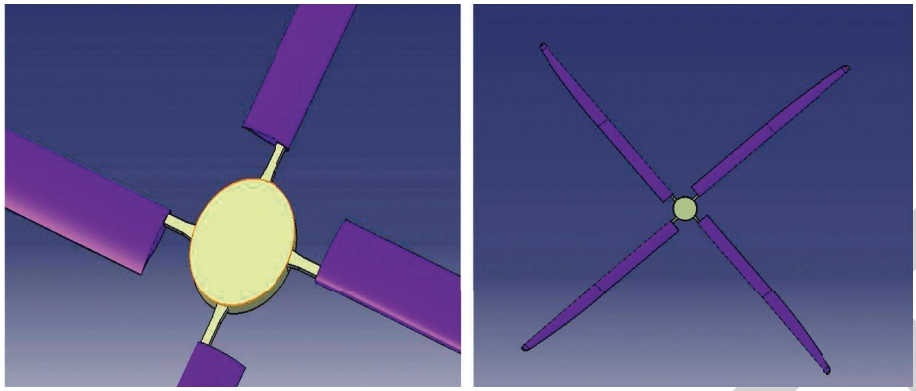

Figure 3: NASA SC(2)-0714 rotor model.

Table 2: Grid independence test.

Domain names	Domain_01	Domain_02	Domain_03	Domain 04
The number of elements	5792001	7055244	10057947	10921474
Lift coefficient	0.89825638	0.99146961	1.0403625	1.0559107
Drag coefficient	0.089324154	0.082220494	0.083640816	0.08252949
Error %	N/A	9.40%	4.69%	1.47%

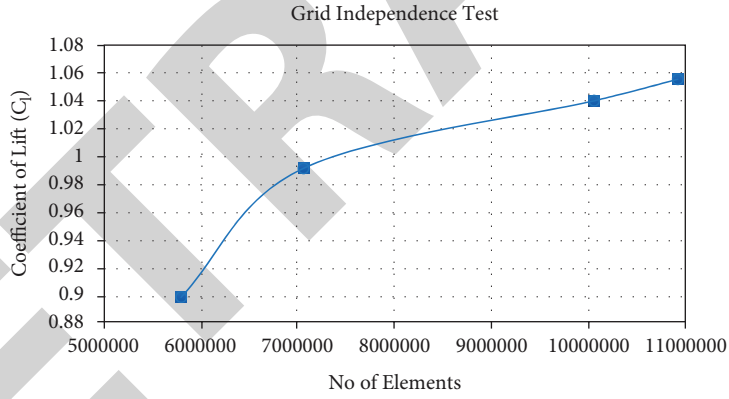

Figure 4: Grid independence test for four-bladed analysis.

In this research, an analysis of an isolated blade was taken. The actual size taken for the analysis in CFD is 12m, but the test section size is 0.6 m × 0.6 m. The model was designed for 500 mm with 200 mm blades and a 100 mm hub for the attachment of blades. A scaled-down model of 1 : 24 size was taken for the analysis in a wind tunnel.

Models were designed using 3D printing techniques. The development of 3D printing technologies helps easy printing and saves time. There are many techniques available for 3D printing. The fusion diffusion modeling (FDM) technique has been used for this research. FDM is a low-cost 3D printing technique in which surfaces will not be smooth. In FDM, the plastic elements are provided with thermal treatment and melted to the required shape. It has less resolution and accuracy. It can be used for basic research purposes. In stereolithography (SLA) techniques, the laser-cured photopolymer resin to obtain the required model. We can select from many materials, and the method is versatile. The model will be very accurate and high resolution. It helps work with prototypes, molds, and patterns. In the selective laser sintering (SLS) technique, polymer powder is fused with laser. It is less costly than SLA and has good mechanical properties [10, 34]. The SLS method is also used for working prototypes and is more expensive than the FDM model. In selective laser melting (SLM), procedures are similar to the SLS technique. In SLM melting, process and materials are different. In SLM, materials are used as a solidified material layer in an entirely molten state. The actual powder layer is completely or partially melted because of the solid laser technique [8].

3D inkjet printing, 3D models are 2D cross section layers by slicing them on a computer. The droplet of the binder

(a) (b)

Figure 5: Wind tunnel and digital indicator for force measurement. (a) Wind tunnel used for testing; (b) force measurement.

NASA SC(2)-0714 ROTOR HH02 ROTOR

Figure 6: 3D printed models used for testing.

material to the powder is applied where the solidification is required as programmed in the computer. Other methods, such as digital light processing (DLP) and carbon DLS technology, are high-cost techniques mainly used for industrial purposes [29].

Pressure and velocity are essential parameters in aerodynamics. In wind tunnels, pressure and velocity are measured with the help of a pitot-static tube and manometer. The pitot-static tube measures total or stagnation pressure and static pressure. Dynamic pressure relates the velocity and pressure, so from the relations, we can find the velocity with the help of pressure [27, 28].

Pressure is related by

$$P_0 = P + \frac{1}{2}\rho V^2. \tag{1}$$

P_0 is the total pressure, and P is the static pressure.

From the above relation, velocity can be found as the pitot-static tube measures total and static pressure.

So, velocity can be found from

$$V = \sqrt{\frac{2(P_0 - P)}{\rho}}. \tag{2}$$

The manometer measures the static pressure and stagnation pressure head using a pitot-static tube. The expression relates to pressure head (H), and pressure is

$$P = \rho g H. \tag{3}$$

So, pressure can be measured by the above relation for stagnation and static pressure. A digital velocity indicator measures velocity, and it is used to calibrate the wind tunnel.

Figures 7 and 8 show the models are fixed inside the wind tunnel test section. Static conditions are measured by

varying the speed in the test section by varying the RPM of the motor. Models are tested at different speeds and validated.

4. Results and Discussion

4.1. Computational Analysis Results. The models were analyzed for Mach numbers 0.3, 0.4, and 0.5. The lift and drag values calculated for HH02 and NASA SC(2)-0714 airfoils gave comparable results to those reported in the literature. The results show that the supercritical airfoil has a better aerodynamic performance than the HH02 airfoil. The lift, drag, and lift-to-drag ratio values are given in Tables 3 and 4 and are represented graphically in Figures 9 and 10. Post-processing results obtained from fluent provided the aerodynamic characteristics of the rotor blade.

The NASA SC(2)-0714 rotor exhibits more lift than the HH02 rotor in comparing lift coefficient. But, drag values are also higher for NASA SC(2)-0714 rotor as we know that induced drag occurs in the flow and causes the higher drag values. In comparing aerodynamic efficiency, the NASA SC(2)-0714 rotor shows much higher efficiency than the HH02 rotor.

The plot between maximum velocity and free-stream Mach number has been plotted. It shows that velocity is always higher for the supercritical airfoil rotor than the HH02 rotor for all three Mach numbers 0.3, 0.4, and 0.5, as shown in Figure 11. From the Velocity values, we can understand that if the velocity is increased, the lift will be increased as the lift is directly proportional to the square of velocity from the basic formula for lift. Similarly, the maximum pressure will be on the lower part of the airfoil from the pressure values, which induces the lift. It proves that NASA SC(2)-0714 airfoil has better lifting capability than HH02 airfoil, as shown in Figure 12.

The maximum pressure and velocity values clearly show that NASA SC(2)-0714 shows high pressure and pressure difference. A high-pressure difference indicates high lift-producing capability for NASA SC(2)-0714 rotors. Similarly, NASA SC(2)-0714 achieves more velocity over the surface. Boundary layers are formed around the blades, but we aim to find the aerodynamic performance of the blades. The effects of the boundary layers are not considered. It is also clear that it increases the critical and drag divergence Mach number and delays the shock creation. Owing to the change in the shape of the trailing edge in the supercritical airfoil, it has different characteristics from the HH02 airfoil. HH02 has a curve aft of the trailing edge at the upper surface, whereas NASA SC(2)-0714 has a curve at the bottom surface of the trailing edge.

In comparing the aerodynamic performance, for Mach number 0.3, the NASA SC(2)-0714 rotor provides 47% better aerodynamic efficiency than the HH02 rotor. Similarly, for Mach number 0.4, the NASA SC(2)-0714 rotor offers 46% better aerodynamic efficiency than the HH02 rotor. Then, for Mach number 0.5,the NASA SC(2)-0714 rotor provides 45% better aerodynamic efficiency than the HH02 rotor. So, in static analysis, the NASA SC(2)-0714 rotor offers superior performance to the HH02 rotor for all speeds.

Figure 7: HH02 rotor model in the wind tunnel.

Figure 8: NASA SC(2)-0714 rotor model in the wind tunnel.

Table 3: Result of HH02 rotor.

4Mach number	0.3	0.4	0.5
The number of elements	12157747	12157747	12157747
Lift coefficient	0.39660177	0.40146145	0.40501018
Drag coefficient	0.058923748	0.055815901	0.054278395
L/D ratio	6.730762782	7.192600008	7.461719898
Max pressure (N/m^2)	4462	7919	12350
Max velocity (m/s)	116.1	154.7	193.2

Table 4: Result of NASA SC(2)-0714 rotor.

4Mach number	0.3	0.4	0.5
The number of elements	10921474	10921474	10921474
Lift coefficient	1.0559107	1.0659764	1.0717936
Drag coefficient	0.08252949	0.080421625	0.078886333
L/D ratio	12.79434418	13.25484781	13.58655624
Max pressure (N/m^2)	5023	8933	13960
Max velocity (m/s)	124.5	166	207

4.2. Wind Tunnel Results. Models are analyzed for static conditions, as shown in Figures 7 and 8. Models are fitted to the three-component balance system attached to the wind tunnel, and the lift force, drag force, and the moment are taken from the force balance system. Readings are tabulated and represented in Tables 5 and 6. Based on the values

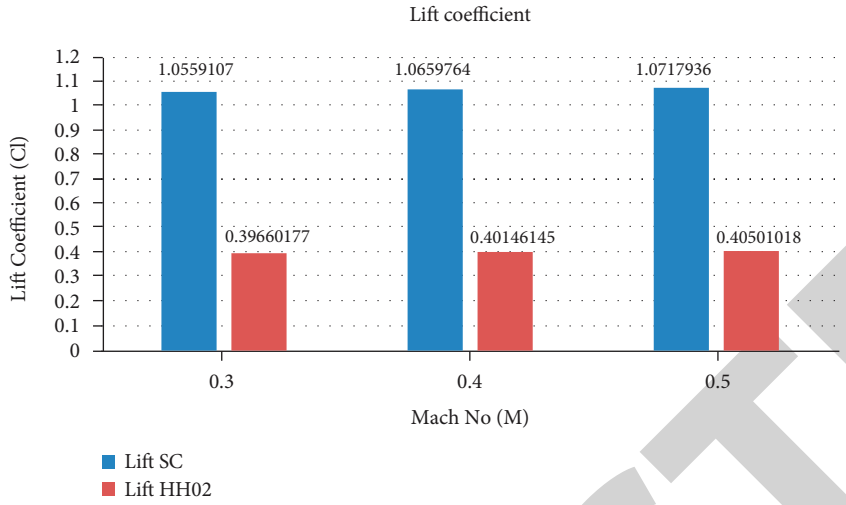

Figure 9: Lift coefficient vs. Mach number.

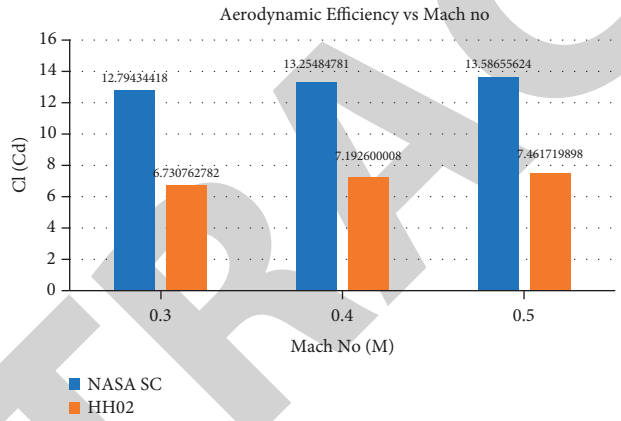

Figure 10: Aerodynamic efficiency vs. Mach no.

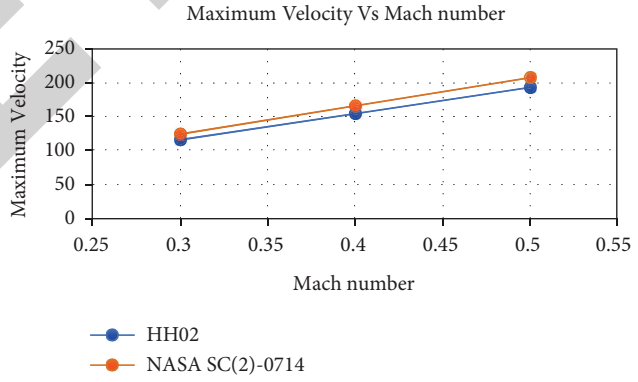

Figure 11: Maximum velocity vs. Mach number.

obtained from wind tunnel testing, aerodynamic efficiency is calculated for NASA SC(2)-0714 and HH02 rotors.

Tables 5 and 6 provide lift, drag, and pitching moment values to show that the NASA SC(2)-0714 rotor produces higher lift, lesser drag, and higher aerodynamic efficiency.

Figures 13 and 14 represent the production of lift force in the wind tunnel for various RPMs for NASA SC(2)-0714 and HH02 rotor models. It clearly shows the velocity increase for an increase in RPM of the wind tunnel rotor fan. Similarly, the lift force is increased for increasing the velocity as the lift

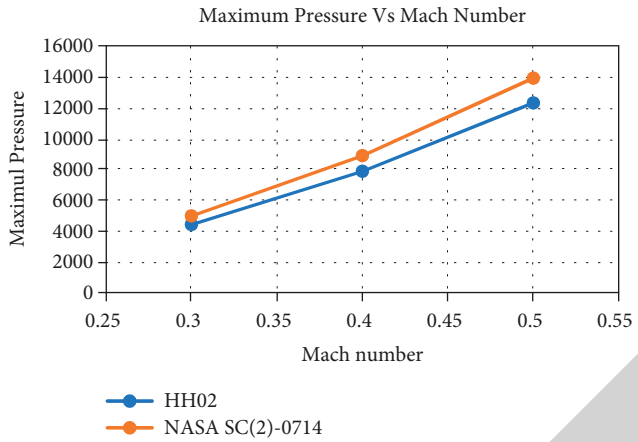

Figure 12: Maximum pressure vs. Mach number.

Table 5: Wind tunnel readings for HH02 model.

S. no.	RPM	Velocity	Lift force	Drag force	Pitching moment	Aerodynamic efficiency (L/D)
1	500	10	2.21	0.2	0.36	11.05
2	600	14	3.28	0.31	0.59	10.58
3	700	19	5.06	0.4	0.89	12.65
4	800	25	7.02	0.56	1.28	12.54
5	900	30	9.45	0.61	1.69	15.49
6	1000	35	11.6	0.75	2.16	15.46

Table 6: Wind tunnel readings for the NASA SC(2)-0714 model.

S. no.	RPM	Velocity	Lift force	Drag force	Pitching moment	Aerodynamic efficiency (L/D)
1	500	10	2.62	0.15	0.43	17.46
2	600	14	4.61	0.25	0.7	18.44
3	700	19	5.77	0.3	1.01	19.23
4	800	25	7.89	0.41	1.42	19.7
5	900	30	10.67	0.5	1.95	20.92
6	1000	35	12.98	0.61	2.48	21.18

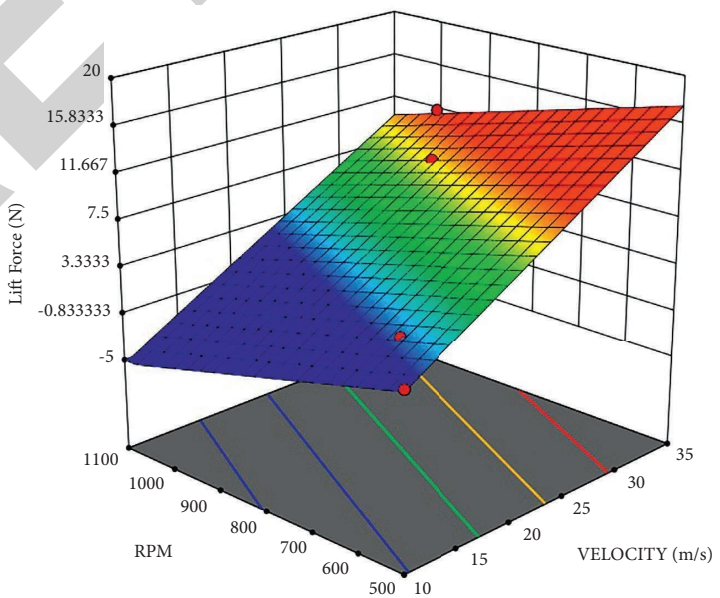

Figure 13: Lift force measured for the HH02 model.

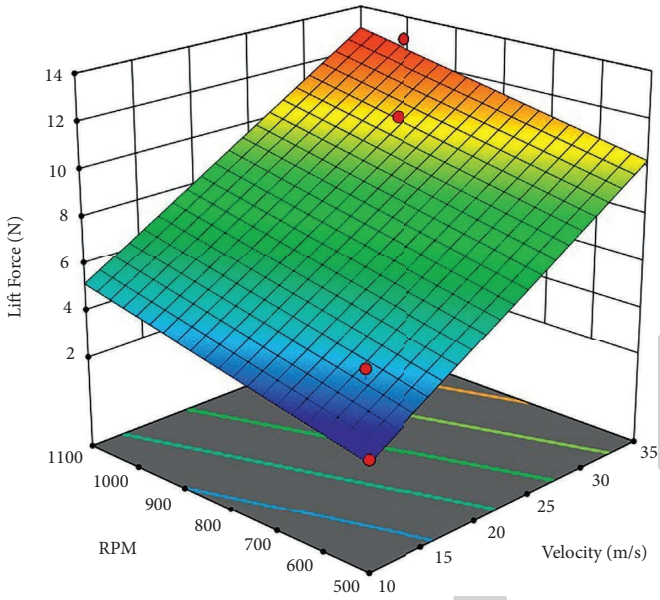

Figure 14: Lift force measured for the NASA SC(2)-0714 model.

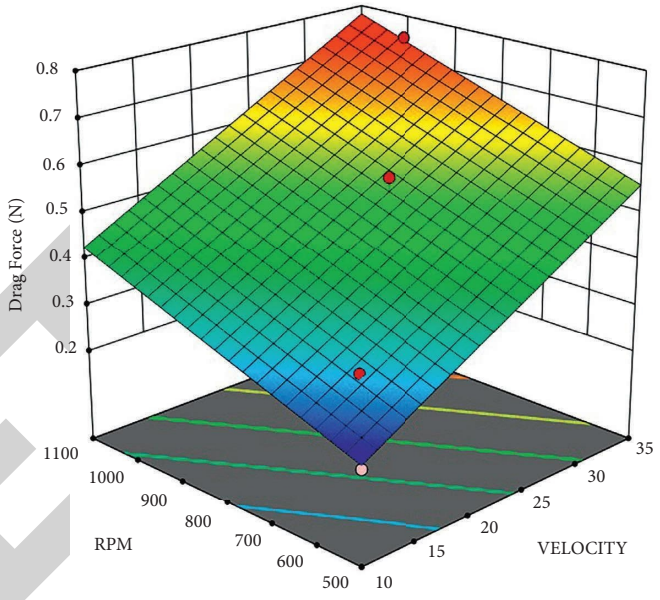

Figure 15: Drag force measured for the HH02 model.

force is proportional to the square of the velocity. In comparing figures, the lift produced in the NASA SC rotor is higher than the HH02 rotor, like the computational analysis results obtained from CFD.

Figures 15 and 16 represent the generation of drag force in the wind tunnel for various RPMs for NASA SC(2)-0714 and HH02 rotor models. It clearly shows that drag force is increased for increasing the velocity as the drag force is proportional to the square of the velocity. In comparing figures and tables, the drag force produced in the NASA SC rotor is lesser than the HH02 rotor, like the computational analysis results obtained from CFD.

Figures 17 and 18 represent the pitching moment measured in the wind tunnel force measurement for the NASA SC rotor and HH02 rotor. It proves that the pitching moment is higher for the NASA SC rotor than the HH02 rotor as it has a higher lift and better aerodynamic efficiency.

A comparison of aerodynamic performance is shown in Table 7.

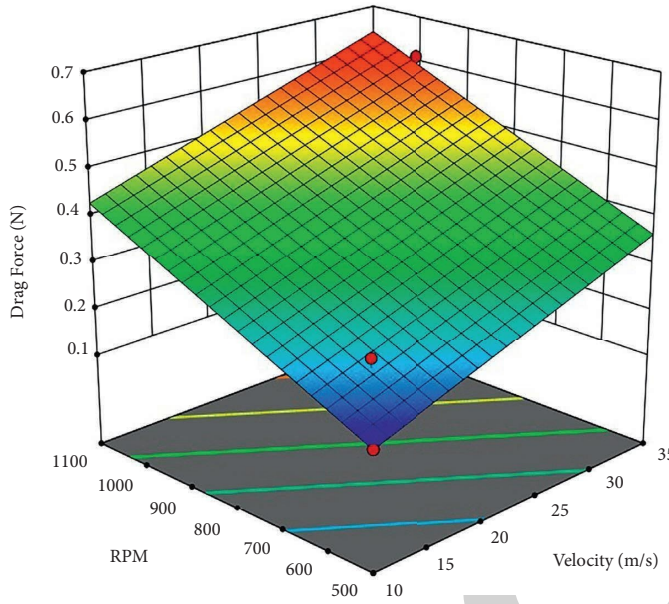

Figure 16: Drag force measured for the NASA SC(2)-0714 model.

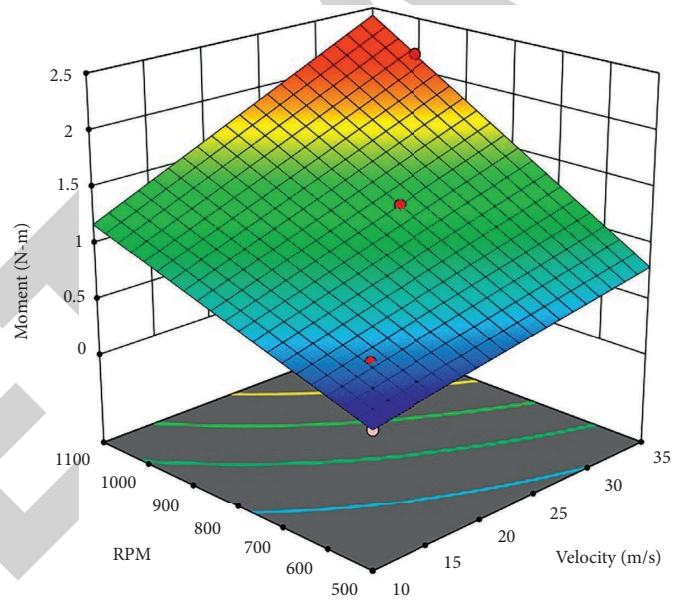

Figure 17: Moment measured for the HH02 model.

The comparison table clearly shows that aerodynamic efficiency for the NASA SC(2)-0714 rotor was better than the HH02 rotor by around 30 to 40% for all speeds. The CFD results obtained for static analysis also showed an improved aerodynamic efficiency of approximately 40%, as discussed in Chapter 4. The experimental data also proved that the NASA SC(2)-0714 rotor provides better aerodynamic performance than the HH02 rotor.

4.3. Validation of Results. For the model's dynamic similarity, force on the model should be equal to the force on the prototype.

Force can be calculated from the relation for dynamic similarity as follows:

$$\begin{aligned}(\text{force})_{\text{prototype}} &= (\text{force})_{\text{model}},\\ F &= m \times a\end{aligned} \tag{4}$$

where "m" is the mass of the body and "a" is the acceleration due to gravity.

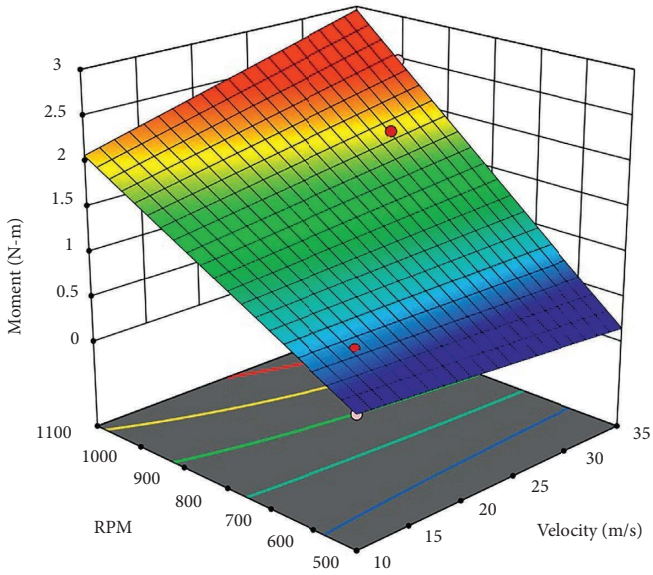

Figure 18: Moment measured for NASA SC(2)-0714 model.

Table 7: Comparison of experimental aerodynamic efficiency.

S. no.	Velocity	L/D NASA SC(2)-0714	L/D HH02	% of improvement
1	10	17.46	11.05	36.71249
2	14	18.44	10.58	42.62473
3	19	19.23	12.65	34.21737
4	25	19.7	12.54	36.34518
5	30	20.92	15.49	25.95602
6	35	21.18	15.46	27.00661

Table 8: Validation of the NASA SC(2)-0714 rotor.

S. no.	Velocity	Exp lift force	CFD lift force	% of error
1	10	1680.599	1980	15.12
2	14	2957.085	3384	12.61
3	19	3701.167	4251	12.93
4	25	5061.041	5754	12.04
5	30	6844.272	7600	9.94
6	35	8326.021	9051	8.01

Table 9: Validation of HH02 rotor.

S. no.	Velocity	Exp lift force	CFD lift force	% of error
1	10	1417.605	1684	15.81
2	14	2103.956	2450	14.12
3	19	3245.737	3751	13.47
4	25	4502.979	5152	12.59
5	30	6061.703	6742	10.09
6	35	7440.82	8201	9.27

Mass flow rate is given as follows:

$$\dot{m} = \rho A V. \tag{5}$$

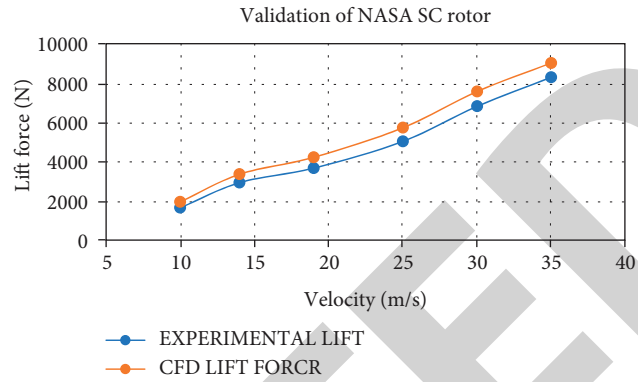

Figure 19: Validation of the NASA SC(2)-0714 rotor.

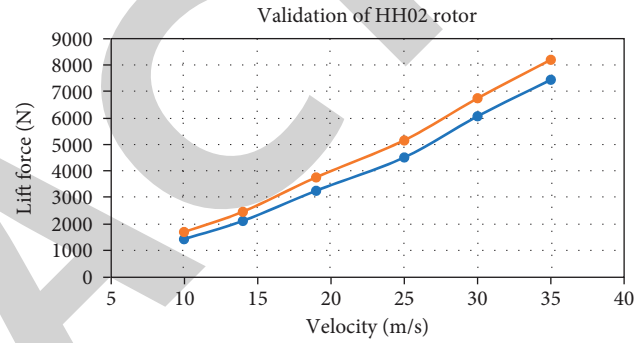

Figure 20: Validation of the HH02 rotor.

From the relation, it can be found that it is a scaled model from 120 cm to 5 cm. The scale ratio is 24.

$$(F)_{\text{prototype}} = 641.45 \times (F)_{\text{model}}. \tag{6}$$

The CFD and experimental values are compared from the calculation of force as in Tables 8 and 9.

The validation of results was mentioned in Tables 8 and 9. It compares the percentage of changes in the CFD and experimental results. It shows that the error percentage is around 15% for lower speed and much lesser at higher speed. It is around 9% for both NASA SC rotor and HH02 rotor. Figures 19 and 20 represent the validation of results and change of nature of the curve for both NASA SC(2)-0714 and HH02 rotors with the CFD and experimental results.

5. Conclusion

The analysis was carried out using the CFD techniques, and the results were validated by wind tunnel testing. Results are validated, and the error percentage is 8% to 15%. Error percentages are within the acceptable limit, and the results are validated with the help of the experimental data. Additive manufacturing techniques are very useful in the aerodynamic testing and validation of models. The computational analysis was successfully validated using an additive manufacturing technique and proved to be the same with acceptable error limits. Error percentage can be minimized by using other methods like SLA or SLS techniques to reduce

the error percentage in experimental results. FDM methods are economical, and it has some roughness over the model. SLS and SLA technique models will have a good finishing and smooth surface. The error in the experimental analysis may be due to the roughness of the FDM method in additive manufacturing. The analysis may be conducted with other additive manufacturing techniques and can be tested in the future for accurate results. Aerodynamic performance can be compared and studied for better additive manufacturing models.

Data Availability

The data used to support the findings of this study are available from the corresponding author upon request.

Conflicts of Interest

The authors declare that there are no conflicts of interest regarding the publication of this article.

References

[1] Petrescu, R. Victoria, R. Aversa et al., "About helicopters," *Journal of Aircraft and Spacecraft Technology*, vol. 1, no. 3, pp. 204–223, 2017.

[2] G. J. Leishman, *Principles of Helicopter Aerodynamics with CD Extra*, Cambridge University Press, Cambridge, UK, 2006.

[3] I. Hasan, R. Mukesh, P. Radha Krishnan, V. Srinath, and R. Dhanya Prakash, "Computational study of aerodynamic performance of three and four-bladed helicopter rotor with supercritical airfoil," *JOURNAL OF ENVIRONMENTAL PROTECTION AND ECOLOGY*, vol. 22, no. 6, pp. 2622–2633, 2021.

[4] J. M. Seddon and N.. Simon, *Basic Helicopter Aerodynamics*, John Wiley & Sons, Hoboken, New Jersey, U.S, 2011.

[5] F. X. Caradonna and T.. Chee, "Experimental and analytical studies of a model helicopter rotor in hover," in *Proceedings of the European Rotorcraft and Powered Lift Aircraft Forum*, Amsterdam, The Netherlands, September, 1981.

[6] A. Brocklehurst and G. N. Barakos, "A review of helicopter rotor blade tip shapes," *Progress in Aerospace Sciences*, vol. 56, pp. 35–74, 2013.

[7] M. Costes, T. Renaud, and B. Rodriguez, "Rotorcraft simulations: a challenge for CFD," *International Journal of Computational Fluid Dynamics*, vol. 26, no. 6-8, pp. 383–405, 2012.

[8] W. L. Oberkampf and T. G. Trucano, "Verification and validation in computational fluid dynamics," *Progress in Aerospace Sciences*, vol. 38, no. 3, pp. 209–272, 2002.

[9] V. F. Kopiev, M. Y. Zaytsev, V. I. Vorontsov, S. A. Karabasov, and V. A. Anikin, "Helicopter noise in hover: computational modelling and experimental validation," *Acoustical Physics*, vol. 63, no. 6, pp. 686–698, 2017.

[10] D. Srinivasan, M. Meignanamoorthy, M. Ravichandran et al., "3D printing manufacturing techniques, materials, and applications: an overview," *Advances in Materials Science and Engineering*, vol. 202110 pages, Article ID 5756563, 2021.

[11] M. R. Ridho, E. A. Agustiany, M. Rahmi Dn et al., "Lignin as green filler in polymer composites: development methods, characteristics, and potential applications," *Advances in Materials Science and Engineering*, vol. 202233 pages, Article ID 1363481, 2022.

[12] S. C. Joshi and A. A. Sheikh, "3D printing in aerospace and its long-term sustainability," *Virtual and Physical Prototyping*, vol. 10, no. 4, pp. 175–185, 2015.

[13] V. Mohanavel, T. Sathish, M. Ravichandran, P. Ganeshan, M. Ravi Kumar, and R. Subbiah, "Experimental investigations on mechanical properties of cotton/hemp fiber reinforced epoxy resin hybrid composites Journal of Physics: conference Series," *Journal of Physics: Conference Series*, vol. 2027, no. 1, Article ID 012015, 2021.

[14] M. Ravichandran, V. Mohanavel, T. Sathish, P. Ganeshan, S. Suresh Kumar, and R. Subbiah, "Mechanical properties of AlN and molybdenum disulfide reinforced aluminium alloy matrix composites Journal of Physics: conference Series," *Journal of Physics: Conference Series*, vol. 2027, no. 1, Article ID 012010, 2021.

[15] T. Raja, S. Ravi, A. Karthick et al., "Comparative study of mechanical properties and thermal stability on banyan/ramie fiber-reinforced hybrid polymer composite," *Advances in Materials Science and Engineering*, vol. 202111 pages, Article ID 5835867, 2021.

[16] I.. Hasan, "Aerodynamic performance analysis of a supercritical airfoil in the helicopter main rotor," *Transactions of the Canadian Society for Mechanical Engineering*, vol. 46, no. 2, pp. 436–458, 2022.

[17] K. M. Pandey and U. Kumar, "Gaurav kumar, dhrubajyoti deka, dipankar das, and anand surana. "CFD analysis of an isolated main helicopter rotor for a hovering flight at varying RPM," *ASME International Mechanical Engineering Congress and Exposition*, vol. 45172, pp. 543–551, 2012.

[18] C. Aumnate, A. Pongwisuthiruchte, P. Pattananuwat, and P. Potiyaraj, "Fabrication of ABS/graphene oxide composite filament for fused filament fabrication (FFF) 3D printing," *Advances in Materials Science and Engineering*, vol. 20189 pages, Article ID 2830437, 2018.

[19] Y. Man, X. Luo, Z. Xie, and D. Qu, "Influence of 3D printed topological structure on lightweight mullite load bearing board in thermal environment," *Advances in Materials Science and Engineering*, vol. 20208 pages, Article ID 8340685, 2020.

[20] I. Hasan, R. Mukesh, P. Radha Krishnan, R. Srinath, and R. B Dhanya Prakash, "Forward flight performance analysis of supercritical airfoil in helicopter main rotor," *Intelligent Automation & Soft Computing*, vol. 33, no. 1, pp. 567–584, 2022.

[21] R. Steijl, G. Barakos, and K. Badcock, "A framework for CFD analysis of helicopter rotors in hover and forward flight," *International Journal for Numerical Methods in Fluids*, vol. 51, no. 8, pp. 819–847, 2006.

[22] S. K. Raman, W. Kexin, T. Ho Kim, A. Suryan, and H. D. Kim, "Effects of flap on the reentry aerodynamics of a blunt cone in the supersonic flow," *International Journal of Mechanical Sciences*, vol. 176, Article ID 105396, 2020.

[23] R. Mukesh, K. Lingadurai, and U. Selvakumar, "Airfoil shape optimization based on surrogate model," *J. Inst. Eng. India Ser. C*, vol. 99, pp. 1–8, 2018.

[24] P. J. Roache, "Quantification of uncertainty in computational fluid dynamics," *Annual Review of Fluid Mechanics*, vol. 29, no. 1, pp. 123–160, 2020.

[25] H. Yamashita, N. Kuratani, M. Yonezawa et al., "Wind tunnel testing on start/unstart characteristics of finite supersonic biplane wing," *International Journal of Aerospace Engineering*, vol. 201310 pages, Article ID 231434, 2013.

[26] C. Zuo, C. Wei, J. Ma, T. Yue, L. Liu, and Z. Shi, "Full-Field displacement measurements of helicopter rotor blades using

stereophotogrammetry," *International Journal of Aerospace Engineering*, vol. 202118 pages, Article ID 8811601, 2021.

[27] X.-kun Jing and Y.-qi Li, "Wind tunnel tests for wind pressure distribution on gable roof buildings," *The Scientific World Journal*, vol. 201311 pages, Article ID 396936, 2013.

[28] R. Mukesh, K. Lingadurai, and U. Selvakumar, "Kriging methodology for surrogate-based airfoil shape optimization," *Arabian Journal for Science and Engineering*, vol. 39, no. 10, pp. 7363–7373, 2014.

[29] D. Balaji, J. Ranga, V. Bhuvaneswari et al., "Additive manufacturing for aerospace from inception to certification," *Journal of Nanomaterials*, vol. 202218 pages, Article ID 7226852, 2022.

[30] J. Zhang, M. Zhang, B. Huang, Y. Li, J. Yu, and F. Jiang, "Wind tunnel test on local wind field around the bridge tower of a truss girder," *Advances in Civil Engineering*, vol. 202113 pages, Article ID 8867668, 2021.

[31] S. Zhang, K. Srividya, I. Kakaravada et al., "A global optimization algorithm for intelligent electromechanical control system with improved filling function," *Scientific Programming*, vol. 202210 pages, Article ID 3361027, 2022.

[32] R. Mukesh, K. Lingadurai, and U. Selvakumar, "Airfoil shape optimization using non-traditional optimization technique and its validation," *Journal of King Saud University-Engineering Sciences*, vol. 26, no. 2, pp. 191–197, 2014.

[33] I. Hasan, G. Ramanan, and V. Manishankar, "Study and comparison analysis of conventional light weight UAV airfoils using XFLR analysis," *ACS Journal for Science and Engineering*, vol. 2, no. 1, pp. 1–9, 2022.

[34] G. Radhaboy, M. Pugazhvadivu, P. Ganeshan, and P. Ramshankar, "Analysis of Thermo chemical behaviour of Calotropis procera parts for their Potentiality," *International Journal of Ambient Energy*, vol. 43, no. 1, pp. 252–258, 2022.